Pergamon

Chaos, Solitons & Fractals Vol. 7, No. 9, pp. 1427–1453, 1996
Copyright © 1996 Elsevier Science Ltd
Printed in Great Britain. All rights reserved
0960-0779/96 $15.00 + 0.00

S0960-0779(96)00006-9

From Annular to Interval Dynamics: Symbolic Analysis of the Periodically Forced Brusselator

JUN-XIAN LIU, WEI-MOU ZHENG and BAI-LIN HAO

Institute of Theoretical Physics, Academia Sinica, P. O. Box 2735, Beijing 100080, China

(Accepted 9 January 1996)

Abstract—In this paper we show that numerical study under the guidance of symbolic dynamics may provide an effective method to gain global knowledge on ODEs, which is difficult to obtain either by purely analytical or by completely numerical means. We demonstrate how this approach works in practice on the example of the periodically forced Brusselator. In particular, the transition from annular type dynamics to interval dynamics is explored in terms of symbolic dynamics. Our results are instructive for the study of other nonlinear systems with competing frequencies, as the method is topological in nature, but complemented with numerical details. Copyright © 1996 Elsevier Science Ltd.

1. INTRODUCTION

Many nonlinear systems are described well by ordinary differential equations (ODEs). When a practitioner in physical science or engineering encounters a set of such equations, it is important to have a global understanding of its bifurcation and chaos 'spectrum': the systematics of periodic orbits, stable as well as unstable ones, at fixed and varying parameters, the type of chaotic attractors which usually occur as limits of sequences of periodic regimes, etc. This is not a simple job to accomplish either by analytical means or by purely numerical study. Recollect the problem of counting the number of limit cycles in planar systems of ODEs. Despite the great effort of mathematicians, it has not been completely solved yet. As chaotic behaviour may appear only in systems of more than three autonomous ODEs or non-autonomous systems with more than two variables, it naturally leads to problems that are much more difficult than counting the number of limit cycles.

Some years ago we suggested associating the systematics of numerically found periodic orbits in ODEs with symbolic dynamics of one-dimensional maps [1]. This was based on the observation that chaotic attractors in many dissipative systems with one positive Lyapunov exponent usually have one-dimension-like structure in some sections. Two systems of ODEs have been studied in detail.

The first system is the periodically forced Brusselator. In fairly large regions of the parameter space the stable periodic orbits may be named and ordered by using a symbolic description of two letters, similar to the symbolic dynamics of the logistic map (for a review see Chap. 5 of [2]). Although there are regions of frequency-locked regimes and transitions from quasiperiodicity to chaos, as to be expected in a driven system, these have not been compared with symbolic dynamics of circle or annular maps.

The second system is the Lorenz model, whose periodic orbits may be systematized by comparing with an antisymmetric cubic map, using a symbolic dynamics of three letters [3]. This study was later extended by invoking symbolic dynamics of two-dimensional maps and antisymmetric map with a discontinuity [4].

While this approach has had some success, many more questions have been raised. We list a few.

1. The number of periodic orbits found in ODEs is usually less than that allowed by the admissibility conditions of the corresponding one-dimensional symbolic dynamics. Within the one-dimensional framework it is hard to tell whether this was caused by insufficient numerical search or by some forbidden rule.
2. In the Poincaré sections of ODEs the attractors often show two-dimensional structures such as layers, bendings, and hooks. On one hand, one has to explain the success of 1D symbolic description, which sometimes even turns out to be better than expected. On the other hand, the limitation of the 1D approach has also to be elucidated, as the Poincaré maps are necessarily two-dimensional.
3. Early effort was more or less concentrated on stable orbits, while unstable orbits play a fundamental role in organizing chaotic motion. It is necessary to develop symbolic dynamics which is capable of treating stable and unstable periodic orbits to some extent alike. Moreover, it is desirable to indicate the structure of some, if not all, chaotic orbits at given parameter set.

Since in the Poincaré sections of ODEs one actually deals with two-dimensional mappings, a significant progress of symbolic dynamics of two-dimensional mappings is required in order to solve the above problems.

The success of symbolic dynamics of one-dimensional maps is largely based on the neat ordering property of real numbers, which is lacking in higher dimensions. This has hindered the development of symbolic dynamics of two-dimensional maps. An essential step forward was the suggestion of Grassberger and Kantz [5] to determine the partition line of the phase plane by connecting 'primary' homoclinic tangencies. Zheng [6] further extended the construction by locating tangencies between the forward contracting foliations and backward contracting foliations, which contains the tangencies between invariant manifolds as subsets. This extension is necessary when knowledge of the partition line in the whole phase plane, not only restricted to the attractor, is required. This happens, for example, when assigning symbolic names to periodic orbits which lie outside the attractor or when treating transient processes. Operationally, this extension also facilitates the determination of partition lines, as the requirement to keep the invariant manifolds disappears.

For one-dimensional mappings, symbolic dynamics has been constructed both in the phase space, e.g. for the ordering of all unstable periodic orbits, and in the parameter space, e.g. by constructing the kneading plane. However, most symbolic dynamics studies on two-dimensional mappings and ODEs have so far been carried out in phase space at fixed parameter values. As in different regions of the parameter space different dynamical regimes may exist, it is of interest to study the transition from one type of symbolic dynamics to another, e.g. from unimodal or Hénon type to circle or annular type. The forced Brusselator turns out to be a good illustration of a general approach, which may also be applied to other planar forced systems.

After introducing the forced Brusselator in Section 2, we develop symbolic dynamics for the dissipative standard map, the two-dimensional counterpart of the circle map in Section 3. This will also help us to fix the terminology of symbolic dynamics of two-dimensional maps. Section 4 studies the forced Brusselator from the viewpoint of the dissipative standard map. Section 5 is devoted to the transition from circle-map type to unimodal-map type behaviour in the Poincaré sections. The process of how symbolic dynamics of three letters reduces to that of two letters is elucidated. Section 6 constructs symbolic dynamics when unimodal or Hénon map captures the essential dynamics on the attractor. Finally, in Section 7, we discuss the general implication of our approach.

2. THE PERIODICALLY FORCED BRUSSELATOR

The term Brusselator was coined by Tyson [7] in 1973 to denote a set of two ODEs, which describe a model of tri-molecular chemical kinetics. The periodically forced Brusselator, first studied by Tomita and Kai [8, 9], is obtained by adding a periodic force to the Brusselator:

$$\begin{aligned} \dot{x} &= A - (B + 1)x + x^2 y + \alpha \cos(\omega t), \\ \dot{y} &= Bx - x^2 y, \end{aligned} \tag{1}$$

where x and y are concentrations of intermediate products, A and B are concentrations of some chemicals under control, α and ω are the forcing amplitude and frequency.

The periodically forced Brusselator (1) is one of the most-studied systems of ODEs. Tomita and Kai [8, 9] discovered a small chaotic region and many periodic 'bubbles' in the $\alpha \sim \omega$ parameter plane. Hao and Zhang, using a subharmonic stroboscopic sampling method [10], explored in great detail the hierarchical structure of chaotic bands and periodic orbits embedded in these bands [11]. This led to the discovery of the first 'universal' ordering of kneading sequences in a system of ODEs [12], so-called U-sequence by Metropolis *et al.* [13] in their study of periodic sequences in unimodal maps. Other findings include intermittent transitions to chaos [14] and transition from quasiperiodic regime to chaos [15].

Figure 1, taken from Ref. [12], shows an $A-\omega$ section of the parameter space for fixed $B = 1.2$ and $\alpha = 0.05$. The solid lines denote boundaries between periodic regimes, and ticked-solid lines are boundaries to period-doubling cascades. The numbers in the figure indicate the periods and Q is the quasiperiodic regime. The dotted regions in Fig. 1 are chaotic with many embedded periodic strips, of which only a few are indicated in the figure. In fact, a method was devised to assign symbolic names to all stable periods, which were found numerically. These words happen to be ordered just as that in the unimodal

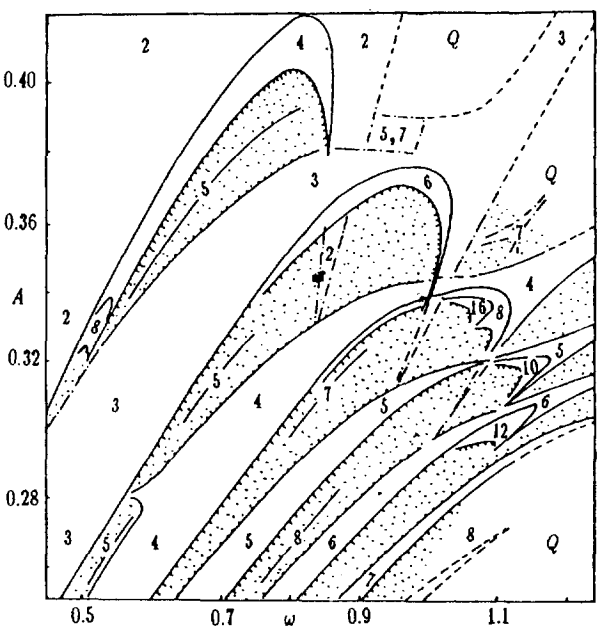

Fig. 1. An $A-\omega$ section in the parameter space with fixed $B = 1.2$ and $\alpha = 0.05$; for details see text.

map. It was along a slanting straight line, say $A = 0.46 - 0.2\omega$ in this plane, where the above U-sequence of MSS [13] was discovered. All but one stable periodic orbits up to period 6, corresponding to those in the unimodal map, exist and are ordered in the same way as in the U-sequence. A large amount of direct numerical search for the only missing period 6 RL^3RC has been in vain. In Section 6 we will show how the absence of this and many other words follows from the admissibility condition of the corresponding two-dimensional symbolic dynamics.

If we cut Fig. 1 along the straight line $A = 0.48 - 0.2\omega$ and take a perpendicular plane, we get an $\alpha - \omega$ section, which is shown in Fig. 2. This is the section where the transition from quasiperiodicity to chaos was first studied in the forced Brusselator [15] and the figure is reproduced from Ref. [2]. In Fig. 2, solid lines denote the boundaries between periodic regimes, and dashed lines are boundaries between periodic and quasiperiodic regions. The numbers indicate periods, Q is the quasiperiodicity and dotted regions are chaotic. We will show that the behaviour of the forced Brusselator in the lower part of this parameter plane is described first by symbolic dynamics of a 1D circle map, then by a 2D symbolic dynamics, similar to that of the dissipative standard map. With increasing α the symbolic dynamics changes first to that of the 2D Hénon map, then to the 1D unimodal map.

3. SYMBOLIC DYNAMICS OF THE DISSIPATIVE STANDARD MAP

Assuming that the symbolic dynamics of 1D circle map is well-known (see, e.g. [16]), we describe its two-dimensional extension, i.e. the dissipative standard map (see also [17]), defined by

$$\begin{aligned} r_{n+1} &= a + br_n + K \sin 2\pi\theta_n, \\ \theta_{n+1} &= \theta_n + r_{n+1} \pmod 1. \end{aligned} \tag{2}$$

The following discussion applies as long as the qualitative behaviour of the first return maps of θ remain the same (see Fig. 5 below), i.e. when the nonlinearity K is kept within a certain range. However, in order to draw the figures, we shall fix the parameters at $a = 0.4$, $b = 0.2$, and $K = 0.334225$.

The Jacobian of the map is

$$J_n = \begin{pmatrix} 1 + 2\pi K \cos 2\pi\theta_n & b \\ 2\pi K \cos 2\pi\theta_n & b \end{pmatrix}. \tag{3}$$

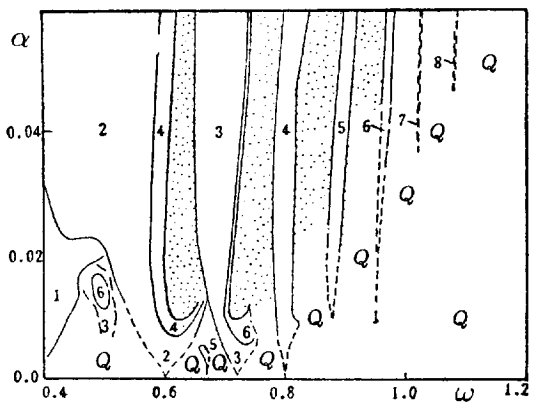

Fig. 2. An α–ω section in the parameter space with $A = 0.48 - 0.2\omega$ and $B = 1.2$.

Consider a point (θ_n, r_n), which has been reached from (θ_{n-j}, r_{n-j}) by iterating (2) j times. The eigenvector corresponding to the larger eigenvalue of the matrix (superscript b is backward)

$$M_n^{\mathrm{b}} \equiv J_{n-1}J_{n-2} \ldots J_{n-j}\tilde{J}_{n-j}\tilde{J}_{n-j-1} \ldots \tilde{J}_{n-1} \tag{4}$$

converges for increasing j, see e.g. [18, 19]. In (4) $\tilde{J}$ denotes the transverse of J. In the $j \to \infty$ limit the eigenvector defines the *unstable direction* at the point (θ_n, r_n). Integral curves of the field of such directions determine the *backward contracting foliation* (BCF) or simply the *backward foliation* of the phase plane. The BCFs are not invariant manifolds in general. However, if a foliation goes through an unstable fixed point or periodic point, then the unstable manifold is a submanifold of BCF. All the points on one and the same backward foliation converge to each other when iterated backward. Therefore, it makes sense to introduce an equivalence relation $\approx$:

$$p_1 \approx p_2 \quad \text{if} \quad \lim_{n\to\infty} |T^{-n}(p_1) - T^{-n}(p_2)| \Rightarrow 0, \tag{5}$$

where $p_i = (\theta_i, r_i)$, and T denotes the map (2).

Similarly, the *stable direction* at (θ_n, r_n) can be found as the $k \to \infty$ limit of the eigenvector, corresponding to the smaller eigenvalue of the matrix (superscript f is forward)

$$M_n^{\mathrm{f}} \equiv \tilde{J}_n\tilde{J}_{n+1} \ldots \tilde{J}_{n+k}J_{n+k}J_{n+k-1} \ldots J_n. \tag{6}$$

The integral curves of such directions determine the *forward contracting foliations* (*FCF*) or simply the *forward foliation* of the phase plane. The FCFs are not invariant manifolds either. If a foliation goes through an unstable fixed point or periodic point, then the stable manifold is a submanifold of FCF. All the points on one and the same forward foliation converge to each other when iterated forward. The equivalence relation is defined as

$$p_1 \approx p_2 \quad \text{if} \quad \lim_{n\to\infty} |T^{n}(p_1) - T^{n}(p_2)| \Rightarrow 0. \tag{7}$$

According to the procedure proposed in Ref. [5] the partition line can be determined from primary tangencies of stable and unstable manifolds of the unstable fixed point. It is natural to extend this procedure to the tangencies between the two classes of foliations [6], thus extending the partition lines into the phase plane beyond the attractor.

In Fig. 3 we show the attractor and two primary partition lines (•S and •G) on the background of the forward foliations (dash curves). The line marked with •D is the preimage of •S. The notations S, G, and D represent Smallest, Greatest, and Discontinuity, as it will be seen in the corresponding first return map (Fig. 5). The areas in between these lines are labelled by •R, •L, and •N.

Since the dynamics takes place on an annulus, we may cut the annulus along the line •S. By dropping (mod 1) in (2) we get the *lifted* (θ, r) plane. In the lifted plane one may take the strip, whose border is the line •S and the line obtained by shifting •S to the right by one unit, to be the fundamental strip. Thus, the area to the left of the •S line in Fig. 3, also marked with •N, belongs to the left neighbour of the fundamental strip. In order to avoid any misunderstanding we note that the partition lines •S and •G are not parallel to the r-axis, as they may seem to be.

Any orbit in the phase plane is coded as a bi-infinite symbolic sequence

$$\ldots s_{-2}s_{-1}\bullet s_0 s_1 s_2 \ldots, \tag{8}$$

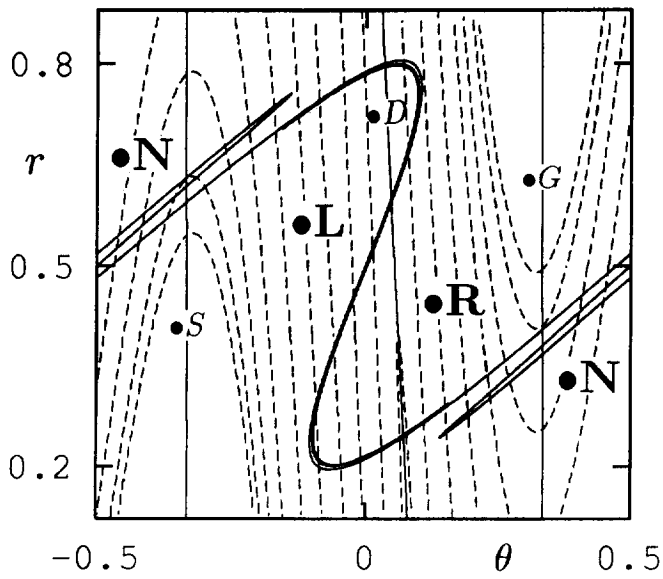

Fig. 3. Two primary partition lines •S and •G of the dissipative standard map. The fundamental strip of the unwrapped annulus is the area between the line •S and its parallel shift to the right by one unit.

where s_i is L, R or N, depending on which area the i-th point of the orbit falls in, and the • indicates the 'present' point. The sequence

$$\bullet s_0 s_1 s_2 \ldots$$

is called the forward symbolic sequence with respect to the present dot (•), and the sequence

$$\ldots s_{-2} s_{-1} \bullet$$

is the backward symbolic sequence.

Another way to partition the phase space is based on preimages, as shown in Fig. 4. Under the inverse map the area marked with L• in the figure will map to the area •L of Fig. 3, while the areas marked with R• and N• map to areas •R and •N in the left strip next to the original one.

We may introduce an ordering in the fundamental strip. According to Fig. 3 we may take

$$\bullet S < \bullet L < \bullet R < \bullet G < \bullet N, \tag{9}$$

and from Fig. 4 it is convenient to have

$$R\bullet < G\bullet < N\bullet < S\bullet < L\bullet. \tag{10}$$

The return map $\theta_{n+1} - \theta_n$, constructed from Fig. 3, is shown in Fig. 5. This map clearly shows two-dimensional features, since it is multi-valued near the discontinuity as well as near the maximum and minimum. However, this does not prevent us from treating it as a one-dimensional map for the following reason. In Fig. 3 all points on one and the same forward foliation (dashed line) have the same future, and, after appropriate coarse-graining, share the same forward symbolic sequence, see eqn (5). Therefore, if we are only interested in forward symbolic sequences, we can shrink different pieces of the attractor along one and the same forward foliation to make it a one-dimensional object.

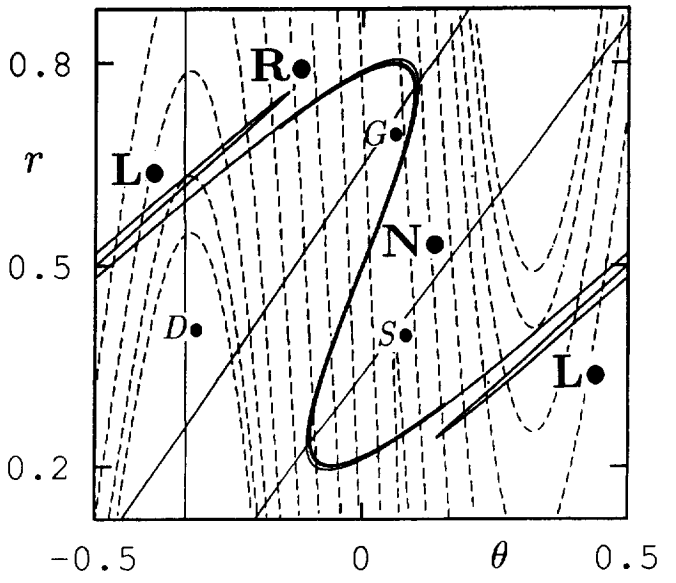

Fig. 4. The partition of the annulus according to pre-images.

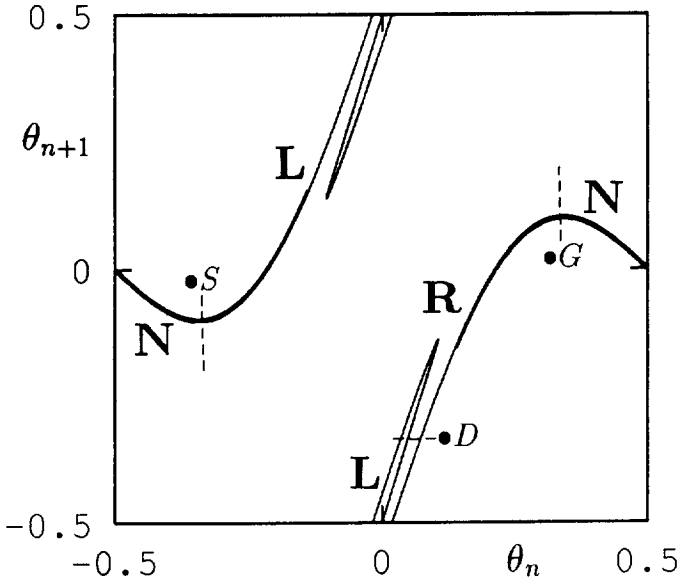

Fig. 5. The $\theta_{n+1} - \theta_n$ first return map.

Reflected in the return map Fig. 5, this means one can neglect the layered structure. Thus in the •N area, variable θ_{n+1} as a function of θ_n is decreasing, while in other areas it is increasing. In other words, only the letter N has an odd parity. We may then extend the ordering rule for symbolic sequences of the circle map to that for the forward sequences of map (2) as

$$\begin{aligned} &\bullet\mathrm{EL}\ldots < \bullet\mathrm{ER}\ldots < \bullet\mathrm{EN}\ldots, \\ &\bullet\mathrm{OL}\ldots > \bullet\mathrm{OR}\ldots > \bullet\mathrm{ON}\ldots, \end{aligned} \tag{11}$$

where E (resp. O) is a finite string consisting of the letters L, R and N, and containing an Even (resp. Odd) number of the letter N.

Similarly, all points on one and the same backward foliation (not shown in Fig. 3 except for the attractor, which is part of the backward foliations) have the same past, and, after appropriate coarse-graining, share the same backward symbolic sequence, see eqn (7). Therefore, based on the ordering (10), backward symbolic sequences are ordered as

$$\begin{aligned} &\ldots \mathrm{RE}\bullet < \ldots \mathrm{NE}\bullet < \ldots \mathrm{LE}\bullet, \\ &\ldots \mathrm{RO}\bullet > \ldots \mathrm{NO}\bullet > \ldots \mathrm{LO}\bullet, \end{aligned} \tag{12}$$

where E and O have the same meaning as in (11).

We can summarize the ordering of symbolic sequences in two-dimensional maps such as (2) as follows. A family of forward foliations are ordered according to their transverse intersections with a backward foliation; a family of backward foliations are ordered according to their transverse intersections with a forward foliation. The order is well-defined as long as there are no tangencies between the two foliations. The occurrence of tangencies is associated with foldings of one family of foliations and with the necessity of introducing a partition line through the tangencies. The ordering reverses on crossing the partition line. In practice, the ordering may be inferred from the local order near a fixed point, i.e. from the signs of the eigenvalues.

As long as foliations are well-ordered, a tangency on a partition puts a restriction on allowed symbolic sequences. For example, when the backward foliations QR• and QN• are tangent to the forward foliation •P on the partition line G•, forming a tangency QG•P, any forward sequence that is greater than •P (geometrically located to the right of the foliation •P) cannot intersect with backward foliations in between QR• and QN•, i.e. with those which are smaller than QN• and greater than QR•. Thus sequences of the type $\mathrm{Q}_+\mathrm{RP}_+$ or $\mathrm{Q}_+\mathrm{NP}_+$ are forbidden by the tangency QG•P, where $\mathrm{Q}_+\bullet > \mathrm{Q}\bullet$ and $\bullet\mathrm{P}_+ > \bullet\mathrm{P}$. Similarly, sequences of the type $\mathrm{U\_NV\_}$ or $\mathrm{U\_LV\_}$ are forbidden by a tangency US•V on the partition line S•, where $\mathrm{U\_}\bullet < \mathrm{U}\bullet$ and $\bullet\mathrm{V\_} < \bullet\mathrm{V}$.

What has been said is best represented in a *symbolic plane* [20]. In order to construct the symbolic plane we introduce a metric representation of symbolic sequences, which embodies the ordering rules (11) and (12). We first define an integer ϵ_i for every symbol s_i:

$$\varepsilon_i = \begin{cases} -1 & \text{if } s_i = N, \\ 1 & \text{otherwise.} \end{cases} \tag{13}$$

We then assign to each forward sequence $\bullet s_1 s_2 \ldots s_i \ldots$ a real number $\alpha \in [0, 1]$:

$$\alpha = \sum_{i=1}^{\infty} \mu_i 3^{-i}, \tag{14}$$

where $\mu_i \in \{0, 1, 2\}$ is defined by

$$\mu_i = \begin{cases} 1 & \text{if } s_i = R, \\ |\epsilon_1 \epsilon_2 \ldots \epsilon_{i-1} - \epsilon_i| & \text{otherwise.} \end{cases} \tag{15}$$

It is easy to see that all forward sequences are ordered according to their α values.

Similarly, we define another integer σ_i for each symbol s_i:

$$\sigma_i = \begin{cases} -1 & \text{if } s_i = L, \\ 1 & \text{otherwise.} \end{cases} \tag{16}$$

and assign to each backward sequence $\ldots s_{-i} \ldots s_{-2} s_{-1}\bullet$ a real number $\beta \in [0, 1]$:

$$\beta = \sum_{i=1}^{\infty} \nu_i 3^{-i}, \tag{17}$$

where

$$\nu_i = \begin{cases} 1 & \text{if } s_{-i} = N, \\ |\epsilon_{-1}\epsilon_{-2} \ldots \epsilon_{-i+1} - \sigma_{-i}| & \text{otherwise.} \end{cases} \tag{18}$$

All backward symbolic sequences are ordered according to their β values.

The unit square $\alpha \in [0, 1] \times \beta \in [0, 1]$ forms the symbolic plane. Horizontal and vertical lines in the symbolic plane correspond to backward and forward foliations, identified by their symbolic sequences, respectively. A point in the unit square represents a bi-infinite symbolic sequence with a given present dot. It can be verified, for example, that in the metric representation we have

$$\begin{aligned} &\alpha(\bullet \mathrm{NL}^{\infty}) = \beta(\mathrm{L}^{\infty}\bullet) = 1, && \alpha(\bullet \mathrm{L}^{\infty}) = \beta(\mathrm{R}^{\infty}\bullet) = 0, \\ &\alpha(\bullet \mathrm{NNL}^{\infty}) = \alpha(\bullet \mathrm{RNL}^{\infty}) = 2/3, && \beta(\mathrm{R}^{\infty}\mathrm{L}\bullet) = \beta(\mathrm{R}^{\infty}\mathrm{N}\bullet) = 2/3, \\ &\alpha(\bullet \mathrm{RL}^{\infty}) = \alpha(\bullet \mathrm{LNL}^{\infty}) = 1/3, && \beta(\mathrm{L}^{\infty}\mathrm{N}\bullet) = \beta(\mathrm{L}^{\infty}\mathrm{R}\bullet) = 1/3. \end{aligned} \tag{19}$$

The two tangencies QG•P and US•V, discussed above, demarcate two 'forbidden zones' in the symbolic plane. Along a partition line an infinite number of tangencies may be found in principle. However, when one is interested in sequences not exceeding a fixed length, a finite number of tangencies is enough. Such a case is shown in Fig. 6, where 20 tangencies are used to outline the forbidden zones. In the figure, 60 000 points representing real orbits are also drawn. All of them are located outside the forbidden zones. Although the image of a forbidden zone is also forbidden, it suffices to consider forbidden zones, formed by primary tangencies. The union of all forbidden zones, determined from one and the same partition line, is called a *fundamental forbidden zone* (FFZ). The boundary of a FFZ is also called a 'pruning front' [20] in the symbolic plane. Therefore, we may say that the

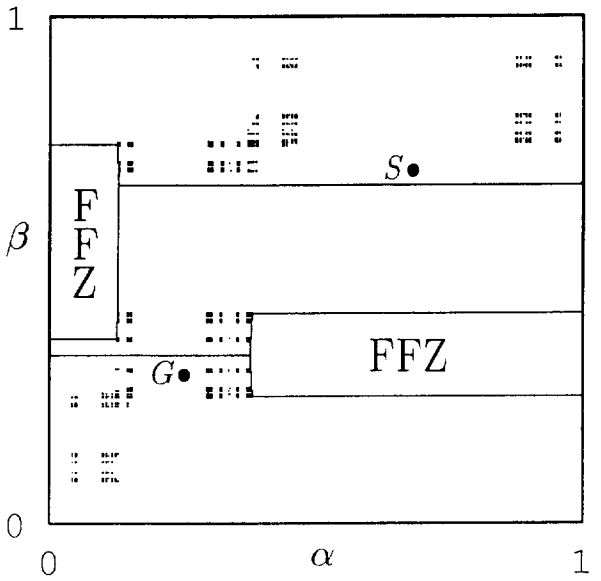

Fig. 6. Symbolic plane of the dissipative standard map. Together with the FFZ, 60 000 points of real orbits are also shown. None of them falls inside the FFZ.

partition lines S• and G• in the phase plane transform into the 'pruning front' in the symbolic plane.

In Fig. 6 the area enclosed by the pruning front of S• and the line $\alpha = 0$ and the area enclosed by the pruning front of G• and the line $\alpha = 1$ form the fundamental forbidden zones (FFZ). Any point within the FFZ corresponds to a forbidden sequence.

Furthermore, from the construction of the FFZ we see that for the tangency QS•P on the line S•, the square enclosed by $\beta = 1$, $\beta = \beta(\text{QL}\bullet)$, $\alpha = 1$ and $\alpha = \alpha(\bullet\text{P})$ does not overlap with the FFZ, thus forming an allowed zone.

If a symbolic sequence has no shifts falling in the FFZ, it is admissible [20]. Therefore, in order to formulate the admissibility conditions for all symbolic sequences an infinite number of tangencies are needed. As long as the role of a single tangency is concerned, it determines a forbidden zone and an allowed zone in the symbolic plane. One can only say that

1. Even if just one shift of a sequence falls in the forbidden zone, the sequence is forbidden.
2. If a sequence has all its shifts in the allowed zone of the given tangency, it is admissible.

In Fig. 7 we sketch the allowed and forbidden zones, formed by four tangencies. A tangency may be compared with a kneading sequence in one-dimensional maps. While a one-dimensional map with a finite number of critical points only possesses a finite number of kneading sequences, a two-dimensional map has infinite many tangencies. However, when we are interested in symbolic orbits not exceeding a finite length, a finite number of tangencies suffice for the job.

We shall rely on the symbolic dynamics of the dissipative standard map to understand the driven Brusselator in the next section. For later comparison of the dissipative standard map with the Poincaré map of the Brusselator it is convenient to map the $\theta - r$ phase plane into the $x - y$ plane by making a transformation

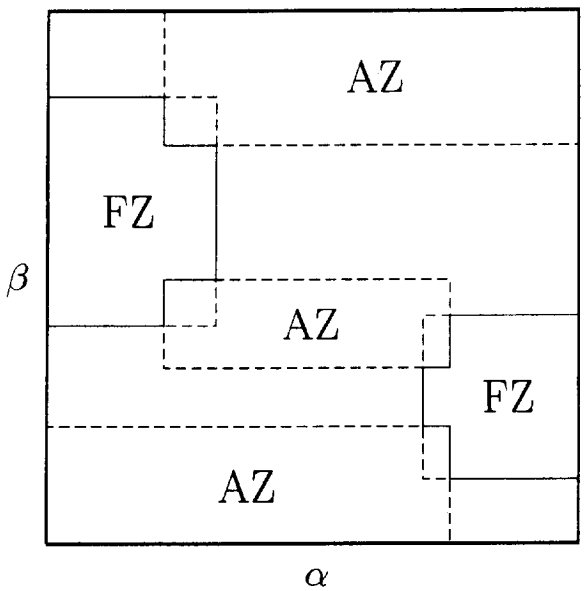

Fig. 7. A sketch of forbidden and allowed zones when two tangencies are used both on S• and G• for the construction.

$$(\theta, r) \to (x, y) = (x_0 - r\cos 2\pi\theta,\ y_0 - r\sin 2\pi\theta).$$

Take $x_0 = y_0 = 1$, the $r - \theta$ plane in Fig. 3 becomes the $x - y$ plane in Fig. 8.

4. THE BRUSSELATOR VIEWED FROM THE STANDARD MAP

The lower part of Fig. 2 looks very much like the parameter plane of a typical circle map. Indeed, quasiperiodic motion and the transition from quasiperiodicity to chaos has been discovered in this region [15]. In order to construct symbolic dynamics we first draw the attractor in the Poincaré section and determine the partition lines. If the attractor does not show much two-dimensional feature, reduction to symbolic dynamics of one-dimensional circle map may capture much of the essentials. We start from this simple case.

Figure 9 shows the chaotic attractor at $\omega = 0.775$, $\alpha = 0.0124$, $B = 1.2$ and $A = 0.48 - 0.2\omega = 0.325$. In order to obtain the stroboscopic portrait an initial phase $t_0 = 0.7\pi/\omega$ is taken. The attractor resembles that of a one-dimensional circle map except for a segment where two sheets are just perceptible. From the tangencies between forward and backward foliations two primary partition lines •G and •S are determined.

Taking the point $(x_r, y_r) = (0.275, 3.64)$ inside the circle as a reference point (which is indicated by a cross in Fig. 9), we define an angle

$$\theta = \frac{1}{2\pi}\tan^{-1}\frac{y - y_r}{x - x_r} + \phi_0$$

for any point (x, y) on the attractor. The phase offset $\phi_0 = 0.225\,826$ is chosen in such a way as to put •S at $\theta \approx 0$. A first return map from θ_n to θ_{n+1}, calculated from Fig. 9, is shown in Fig. 10. The three monotone segments in Fig. 10 may be assigned the letters L, R, and N, in accordance with the two-dimensional partitions in Fig. 9.

Many tangent points may be identified on the partition line S•. It turns out that all the

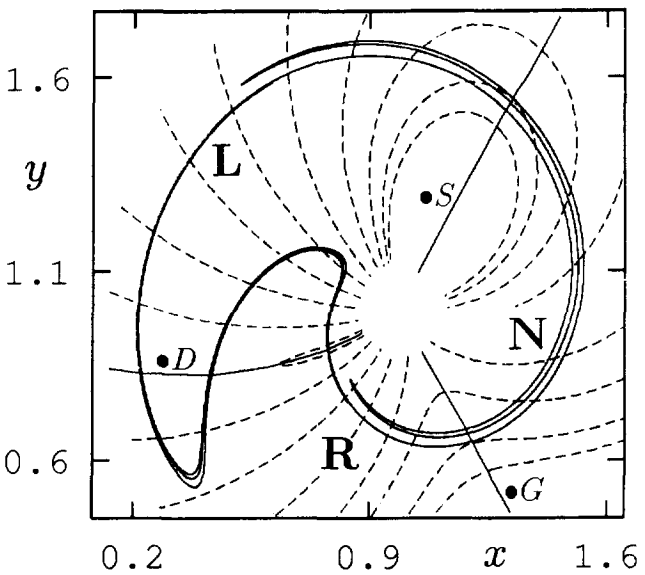

Fig. 8. Attractor in the dissipative standard map, shown in the x–y plane instead of the r–θ plane, cf. Fig. 3.

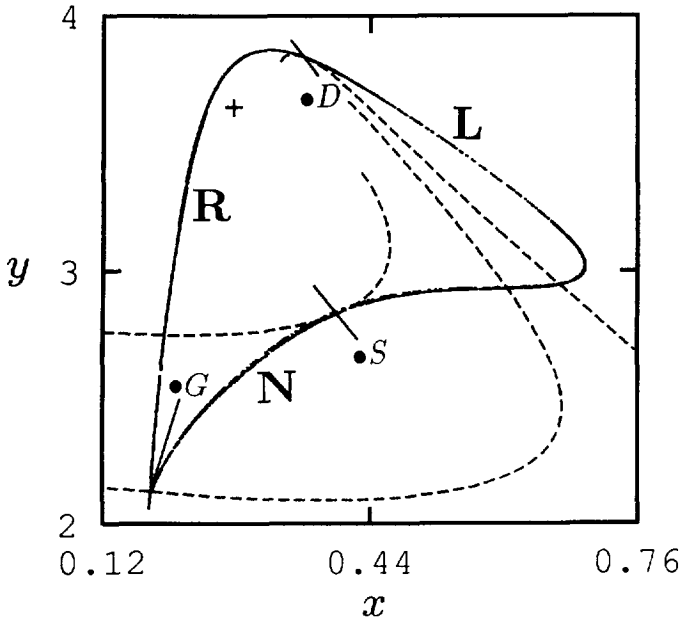

Fig. 9. A Poincaré section at $\omega = 0.775$, $A = 0.325$, $B = 1.2$, and $\alpha = 0.0124$. The partition lines •S, •G, and the pre-image •D of •S divide the attractor into three parts, denoted by the letters L, R, and N.

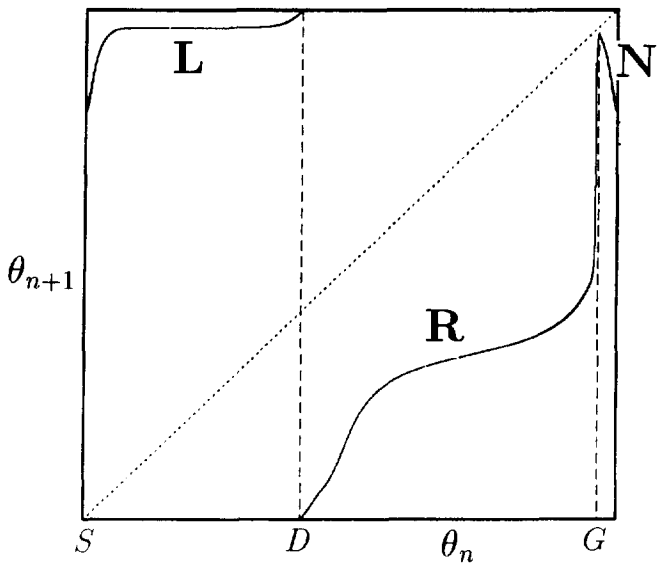

Fig. 10. The first return map obtained by mapping the attractor in Fig. 9 to the $\theta_n - \theta_{n+1}$ plane.

forward symbolic sequences for attractor points have at least 11 leading letters in common. For example, two points are

T_1: . . . LLLLRLRRLRRLRRNRDS•RLNRRLRRLNRLNRRLRRLN . . .,

T_2: . . . RRRRRRRRRRRRRRRRDS•RLNRRLRRLNRRLRRRLRRL . . ..

On the line G• the common leading string of all forward sequences are determined to be at least 16 letters long. Two of these tangencies are

$$T_3\text{: . . . RLRLRRLRLRRLRLRRLG•RRLRRRLRRRLRRRLRLNRR . . .,}$$

$$T_4\text{: . . . RRRRRRRRRRRRRRRRLG•RRLRRRLRRRLRRRLRRLNR . . ..}$$

In reducing the two-dimensional attractor to one-dimensional return map, we should pick out the smallest forward sequence among all tangencies at S• to be the kneading sequence K_S, and pick out the greatest forward sequence among all tangencies at G• to be the kneading sequence K_G. Among all the tangencies we have determined these are T_1 and T_4, respectively.

$$\begin{aligned} K_S &= T_1 = \text{RLNRRLRRLNRLNRRLRRLN . . .,} \\ K_G &= T_4 = \text{RRLRRRLRRRLRRRLRRLNR . . ..} \end{aligned} \tag{20}$$

Compared with the original 2D map, the 1D circle map given by these K_S and K_G puts less constraints on allowed orbits. Since on either partition line the common leading string of forward sequences is quite long (over 11 or 16 letters) no difference between the 1D and 2D maps can be recognized if only periodic orbits with periods shorter than 11 are concerned.

The knowledge of the two kneading sequences (20) determines everything in the symbolic dynamics of the circle map [16]. For example, one may define a *rotation number* W, also called a *winding number*, for a symbolic sequence by counting the weight of letters R and N, i.e. those on the right branch of the first return map, in the total number n of all letters:

$$W = \lim_{n\to\infty} \frac{1}{n}(\text{number of R and N}). \tag{21}$$

A chaotic regime is associated with the existence of a rotation interval, a closed interval in the parameter plane [21]. Within a rotation interval there must be well-ordered orbits. We can construct some of these well-ordered sequences explicitly, knowing the kneading sequences K_S and K_G.

In our case it can be verified that the ordered periodic orbits $(RRL)^\infty$ and $[(R^3L)^3R^2L]^\infty$ are admissible. These two sequences have rotation numbers 2/3 and 11/15, so the rotation interval of the circle map contains [2/3, 11/15], inside which there are rational rotation numbers 5/7, 7/10, 8/11, and 9/13 with denominators less than 15. Their corresponding ordered orbits are $(R^3LR^2L)^\infty$, $[R^3L(R^2L)^2]^\infty$, $[(R^3L)^2R^2L]^\infty$, and $[R^3L(R^2L)^3]^\infty$. (For a simple graphical method to construct symbolic sequence from a rational rotation number see Fig. 4.8 in Ref. [2].)

We can further construct sequences which are not well-ordered from well-ordered ones by the following transformation. One notes that the left limit of the point D is the greatest point on the subinterval L, while the right limit of D is the smallest R. When the point D is crossed by a continuous change of initial points the corresponding symbolic sequences must change as follows:

$$\text{greatest LN . . . } \rightleftharpoons \text{ smallest RL . . ..}$$

Similarly, on crossing the critical point G another change of symbols takes place:

$$\text{greatest R} \rightleftharpoons \text{smallest N.}$$

Neither change has any effect on rotation numbers. As an example, starting with the ordered period 7 orbit $(R^3LR^2L)^\infty$ we obtain

$$\text{LRRLRRR} \rightarrow \text{LRRLNRR} \rightarrow \text{LNRLNRR} \rightarrow \text{LNRLNNR}$$

as candidates for the fundamental strings in not well-ordered sequences of period 7. Among the four sequences, the latter two are forbidden by K_G.

In this way we have determined all periodic sequences up to period 15, allowed by the two kneading sequences (20). The result is summarized in Table 1. We have examined the admissibility of all these sequences by using the four tangencies T_1–T_4. They are all allowed. In fact, we have numerically found all these orbits in the Brusselator.

A more interesting case is encountered at $\omega = 0.66$ and $\alpha = 0.0145$. The attractor and the primary partition lines are shown in Fig. 11, which manifestly shows two-dimensional features. From the tangencies along the S• and G• lines we list the following seven:

T_1: . . . RRRRRRRRRRRRRLRDS•LNRLRLRLLNRLRRLRRLLN . . .,

T_2: . . . RRRRRRRRRLRLRLNDS•LNRLRLRLRLRLRRLRRLRR . . .,

T_3: . . . RRRRRRRRRRRRRRLDS•LNRLRLRRLRRLRLRRLRRL . . .,

T_4: . . . RRRLRLRLRLRLLNRLDS•LNRLRRLRLRLRRLRRLRRL . . .,

T_5: . . . RRRLRLRLRLRLRLRLDS•LNRLRRLRRLRLNRLLNRLR . . .,

T_6: . . . RRLRLRLRLRLRLRLLLG•RLRRLRRLRRLLNLNRLRLR . . .,

T_7: . . . RRRRRRRRRRRRRRRLG•RLRRLRRLRRLRLLNLNLNL . . ..

Picking out the smallest forward sequences along S• and the greatest one along G•, we get

$$K_S = T_5 = \text{LNRLRRLRRLRLNRLLNRLR} \ldots,$$

$$K_G = T_7 = \text{RLRRLRRLRRLRLLNLNLNL} \ldots.$$

For the 1D circle map, we have determined all allowed periodic sequences up to period 11, which are listed in Table 2. Some of these cycles are now forbidden by certain tangencies of the 2D Poincaré map. For example, among the four sequences of period 7 the cycle $(\text{NRLRLNL})^\infty$, denoted by an asterisk in Table 2, is forbidden by the tangency T_2 since the shift $(\text{LNRLRLN})^\infty \bullet (\text{LNRLRLN})^\infty$ is in the forbidden zone of T_2. There are

Table 1. Allowed periodic sequences up to period 15 for the circle map corresponding to $\omega = 0.775$ and $\alpha = 0.0124$

P	W	Sequences
3	2/3	RLR RLN
6	2/3	RRLRLN
7	5/7	RRLRRLR RRLRRLN
9	2/3	RRLRLNRLN RRLRRLRLN
10	7/10	RRLRRLRRLR RRLRRLRRLN
11	8/11	RRLRRRLRRLR RRLRRRLRRLN
12	2/3	RRLRRLRLN RRLRRLRRLRLN RRLRLNRLNRLN
13	9/13	RRLRRLRRLRRLR RRLRRLRRLRRLN RRLRRLRRRLRLN RRLRRLRRLNRLN
14	5/7	RRLRRRLRRLRRLR RRLRRRLRRL RRLN RRLRRLN RRLRRLR
15	11/15	RRLRRRLRRRLRRLR RRLRRRLRRRLRRLN

Only non-repeating strings of the sequences are given. P denotes the period and W the rotation number.

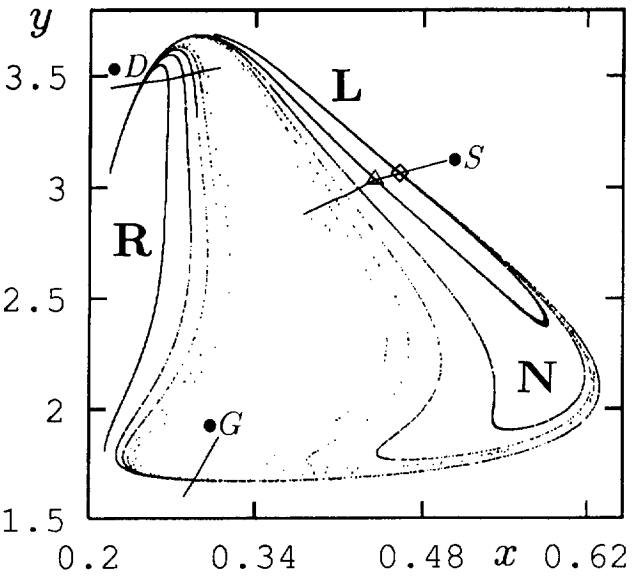

Fig. 11. A Poincaré section at $\omega = 0.66$, $A = 0.348$, $B = 1.2$, and $\alpha = 0.0145$.

Table 2. Allowed periodic sequences up to period 11 for the 1D circle map corresponding to $\omega = 0.66$ and $\alpha = 0.0145$

P	W	Sequences
2	1/2	RL NL
4	1/2	NRLL
5	3/5	RRLRL NRLRL
6	1/2	NRLRLL NLNRLL
7	4/7	RRLRLRL NRLRLRL RRLLNRL NRLRLNL†
8	1/2	NRLRLRLL NLNRLRLL NRLLNLNL
8	5/8	RRLRRLRL NRLRRLRL
9	5/9	RRLRLRLRL NRLRLRLRL RRLLNRLRL† NLNRLRLNL†
9	5/9	NRLRLRLNL† NRLRRLLNL NRLRRLRLL NRLRLNRLL†
10	1/2	NRLLNLNLNL NRLLNLNRLL NRLRLLNLNL NRLLNRLRLL
10	1/2	NRLRLRLRLL NRLRLRLLNL
11	6/11	RRLRLRLRLRL NRLRLRLRLRL NLNRLRLRLRL NRLRLRLRRLL
11	6/11	NRLLNRLRLRL NLNLNRLRLRL NRLRLRRLRLL NRLRLLNRLRL
11	6/11	NRLRRLRLRLL NRLLNLNRLRL NLNLNLNRLRL NLNRLLNRLRL
11	6/11	NRLLNRLRRLL
11	7/11	RRLRRLRRLRL NRLRRLRRLRL

†Forbidden by 2D tangencies.

four forbidden sequences of period 9. All other cycles up to period 9 are allowed. We have examined their admissibility and found all of them numerically. Compare the symbolic plane Fig. 6 of the dissipative standard map with the symbolic plane of the Brusselator shown in Fig. 12. The two figures look similar.

So far we have discussed only periodic orbits. In principle, the admissibility of any given orbit can be examined. Although it is impossible to construct all admissible chaotic sequences, we are able to tell the structure of some chaotic orbits. For instance, a chaotic sequence may be obtained by randomly linking the segments LR and LLRR, as it can be

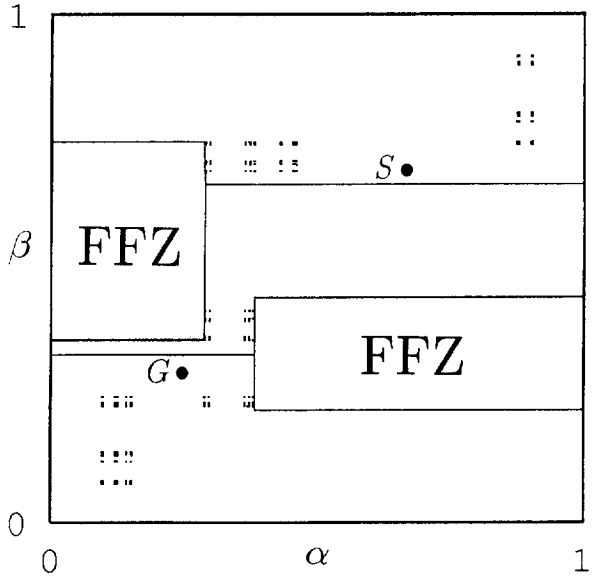

Fig. 12. The symbolic plane of the attractor in Fig. 11. Together with the FFZ, 70000 points of real orbits are shown, none of which falls inside the FFZ.

verified that all shifts of such a sequence fall in the allowed zone of the tangency T_1 or T_6. Furthermore, from the tangencies T_1 and T_6 it follows that any sequence consisting of only the segments RL and LN is also admissible.

5. TRANSITION FROM ANNULAR TO INTERVAL DYNAMICS

When the nonlinear coupling α in the forced Brusselator (1) increases, the dynamics undergoes a transition from annular type to that of an interval. It is interesting to trace the change of the corresponding symbolic dynamics from circle type to unimodal type, in particular, to watch how the number of symbols reduces from three to two. In the free Brusselator there is a Hopf bifurcation, where the stable fixed point at $(x, y) = (A, B/A)$ loses stability and a limit cycle comes into being. All the rich dynamical behaviour of the forced Brusselator appears as the interaction between the limit cycle and the linear oscillator $\cos(\omega t)$ changes. Therefore, it is normal to expect that the nature of the unstable fixed point plays an essential role in the transition under study.

Roughly speaking, the transition undergoes the following stages:

1. For a small enough α, the fixed point is an unstable focus, i.e. both eigenvalues are complex with moduli bigger than 1. The phase portrait is an 1D closed curve and the return map $\theta_{n+1} - \theta_n$ is a subcritical circle map without any decreasing branch. The symbolic dynamics is that of rigid rotation, i.e. with two letters of even parity.
2. At a first critical α_{c1} the circle map undergoes a transition from subcritical to supercritical regime. While the fixed point remains an unstable focus, the backward and forward foliations begin to show tangencies. This signals the appearance of a decreasing branch in the return map, requiring a third letter with odd parity to construct the symbolic dynamics.
3. Upon further increase of α the fixed point becomes an unstable node, i.e. the two eigenvalues both become real with moduli greater than 1. The phase portrait and first

return map show two-dimensional feature clearly, e.g. multi-layered structure. However, a standard-map type symbolic dynamics still works well.

4. When the modulus of one of the eigenvalues becomes less than 1, the fixed point becomes a saddle. The predominant motion changes from rotational to vibrational. The 'return plot' in terms of $\theta_{n+1}-\theta_n$ can no longer be treated as a one-dimensional map. However, the phase portrait and the $y_{n+1}-y_n$ or $x_{n+1}-x_n$ return map may be analysed by using a Hénon type symbolic dynamics.
5. Further decrease of the smaller eigenvalue makes the attractor and the $y_{n+1}-y_n$ return map even more close to one-dimensional. The dynamics fits well into that of a unimodal map.

These stages are demonstrated in Fig. 13, where we have collected the phase portraits of the attractor, the $\theta_{n+1}-\theta_n$ and $x_{n+1}-x_n$ return maps, at five different α values along the vertical line $\omega = 0.775$ in Fig. 2.

The $\alpha = 0.0124$ case (top row in Fig. 13) has been discussed in detail in Section 4 (see Fig. 9). In fact, it is representative for a wide range of α, say, from 0.006 to 0.0154. The $\theta_{n+1}-\theta_n$ return map is essentially a one-dimensional circle map.

At $\alpha = 0.027$ the fixed point is an unstable node with eigenvalues $\lambda_1 = -1.442\,634$ and $\lambda_2 = -1.262\,673\,4$ (2nd row in Fig. 13). The two-dimensional feature of the attractor and the $\theta_{n+1}-\theta_n$ return map calls for symbolic dynamics analysis, similar to that of the dissipative standard map. However, after shrinking along the forward foliations, symbolic dynamics of a one-dimensional circle map still captures the essentials.

Once the fixed point has become a saddle, e.g. at $\alpha = 0.05$, $\lambda_1 = -2.522\,606\,7$ and $\lambda_2 = -0.495\,022\,4$ (3rd row in Fig. 13), the dynamics is no longer annular type and Hénon type symbolic dynamics must be developed, as will be done in Section 6.

Due to the change of the dynamics to interval type, the $\theta_{n+1}-\theta_n$ return maps for greater values of α are of no use. Now the $x_{n+1}-x_n$ or $y_{n+1}-y_n$ return maps should be used instead. If the $\alpha = 0.08$ case still needs two-dimensional consideration, the $\alpha = 0.2$ case (last row in Fig. 13) turns out to be one-dimensional to high precision. This explains our early success in applying purely one-dimensional symbolic dynamics to the study of the forced Brusselator.

An interesting, but open question is the connection between the three letters used in annular type symbolic dynamics and the two letters used in Hénon type maps. It is a prerequisite for the clarification of the relation between the Farey sequence in circle map and the U-sequence in unimodal map and requires further investigation.

6. SYMBOLIC ANALYSIS OF INTERVAL DYNAMICS

Now we turn to symbolic dynamics analysis of the forced Brusselator when the interval dynamics predominates. This happens, e.g. at the $\alpha = 0.05$ level in Fig. 2, i.e. along the $A = 0.48 - 0.2\omega$ or $A = 0.46 - 0.2\omega$ slanting lines in Fig. 1. In Fig. 14 we show a $y - \omega$ bifurcation diagram of the Brusselator along the $A = 0.46 - 0.2\omega$ line in Fig. 1. It is nothing but a plot of the y projection of the Poincaré section against the parameter ω.

Only when the dynamics is controlled by a saddle-type unstable fixed point, the symbolic dynamics is close to that of a mapping on an interval. This is the case, e.g. at $\omega = 0.705$ and its vicinity, within the second chaotic band shown in Fig. 14.

Figure 15 shows the chaotic attractor in the background of the FCF (dashed lines) and the BCF (dotted lines). The attractor, of course, is part of the BCF. The partition line C• is determined from tangencies between FCF and BCF. From the tangencies along C• we

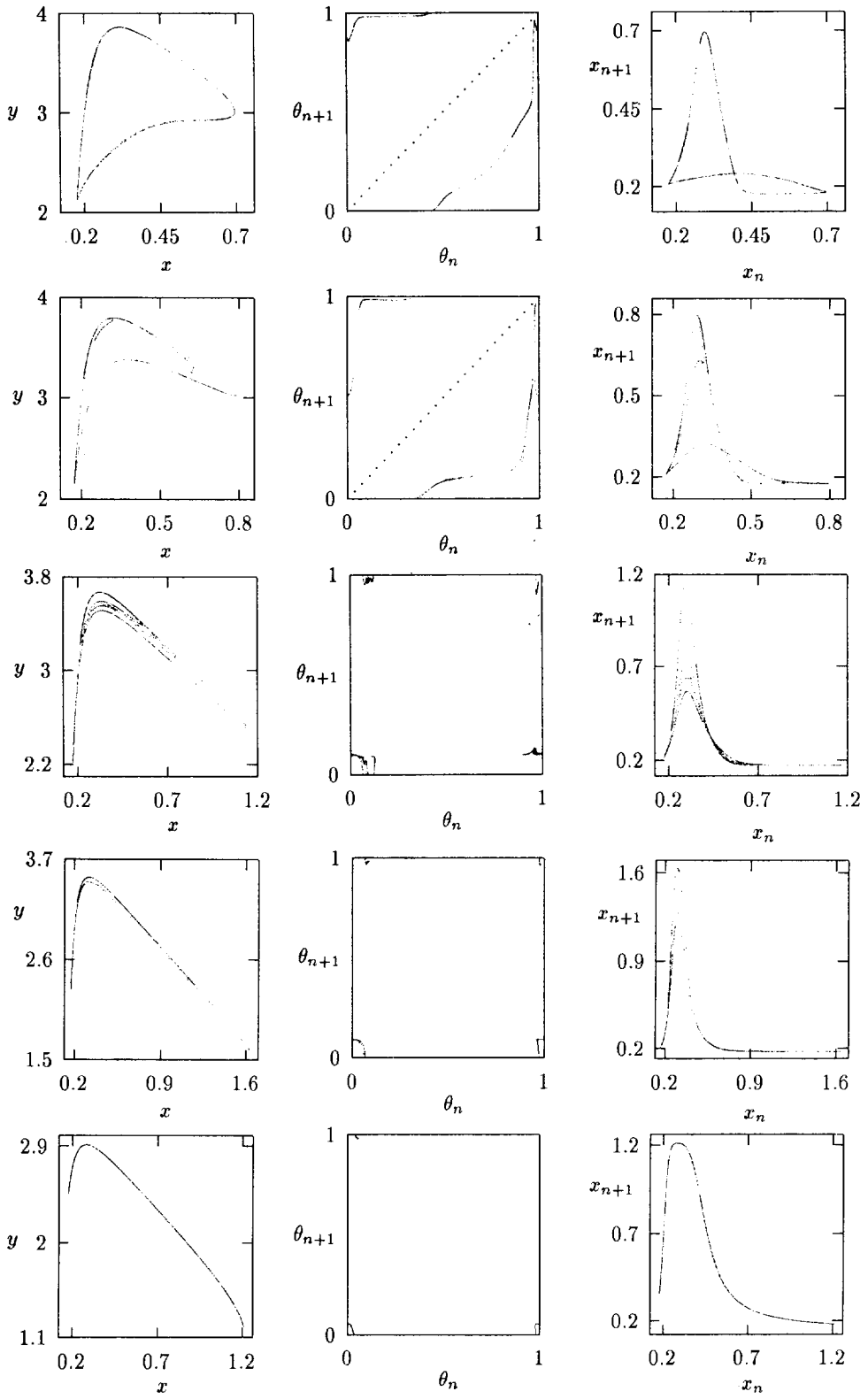

Fig. 13. Transition from annular to interval dynamics. Phase portraits of the attractor, $\theta_{n+1} - \theta_n$ return maps, and $x_{n+1} - x_n$ return maps are juxtaposed at five different α values for $\omega = 0.775$ and $A = 0.48 - 0.2\omega = 0.325$. From top to bottom: $\alpha = 0.0124$, 0.027, 0.05, 0.08, and 0.2.

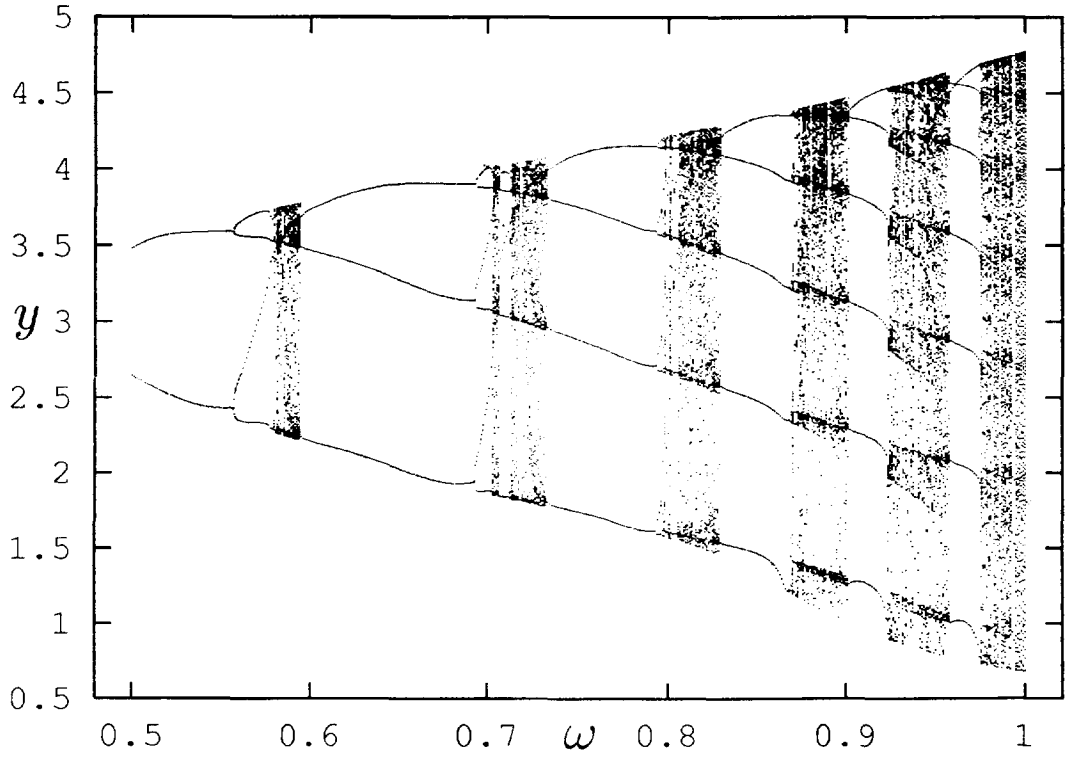

Fig. 14. The $y-\omega$ bifurcation diagram for the forced Brusselator along the $A = 0.46 - 0.2\omega$ line in Fig. 1.

choose the following six, which are enough to examine the admissibility of orbits no greater than $(RLLRC)^\infty$:

T_1: $L^\infty RC\bullet RL^2RLRL^2RLR^2L^2RLRLRL^2RLRL^2RL^2R$ . . . (0.289 703 116 3, 3.530 402 964 7)

T_2: $L^\infty R^5C\bullet RL^2RLRL^2RLR^2L^2RL^2RLRL^2RL^2RLRLR$ . . . (0.280 061 221 1, 3.525 107 243 4)

T_3: $L^\infty R^4C\bullet RL^2RLRL^2RLR^2LR^5L^2RLRL^2RLR^2L$ . . . (0.278 167 618 7, 3.523 878 696 3)

T_4: $L^\infty R^2LR^2C\bullet RL^2RLRL^2RLR^2LRL^2RLRL^2RL^2RLR^2L^2$ . . .
(0.276 691 028 1, 3.522 904 458 4)

T_5: $L^\infty R^2C\bullet RL^2RLRL^2RLR^3L^2RLRLRL^2RL^2RLRL^2$ . . . (0.261 770 524 8, 3.513 294 263 7)

T_6: $L^\infty C\bullet RL^2RLRL^2RLR^3L^2RLRLR^2L^2RL^2RLR^2$ . . . (0.261 306 747 0, 3.512 490 519 5)

where C stands for either R or L. We have given the precise locations of the tangencies for each.

Once a partition line has been determined, each orbit may be encoded with a doubly infinite symbolic sequence like the one shown in (8). However, now it consists of only two letters, R and L. Accordingly, the metric representation of symbolic sequences is somewhat simpler as defined below.

We assign an integer $\epsilon_i = 1$ or -1 to a symbol s_i when it is L or R. To each forward sequence $\bullet s_1 s_2 \ldots s_n \ldots$ we assign a real number α:

$$\alpha = \sum_{i=1}^{\infty} \mu_i 2^{-i}, \tag{22}$$

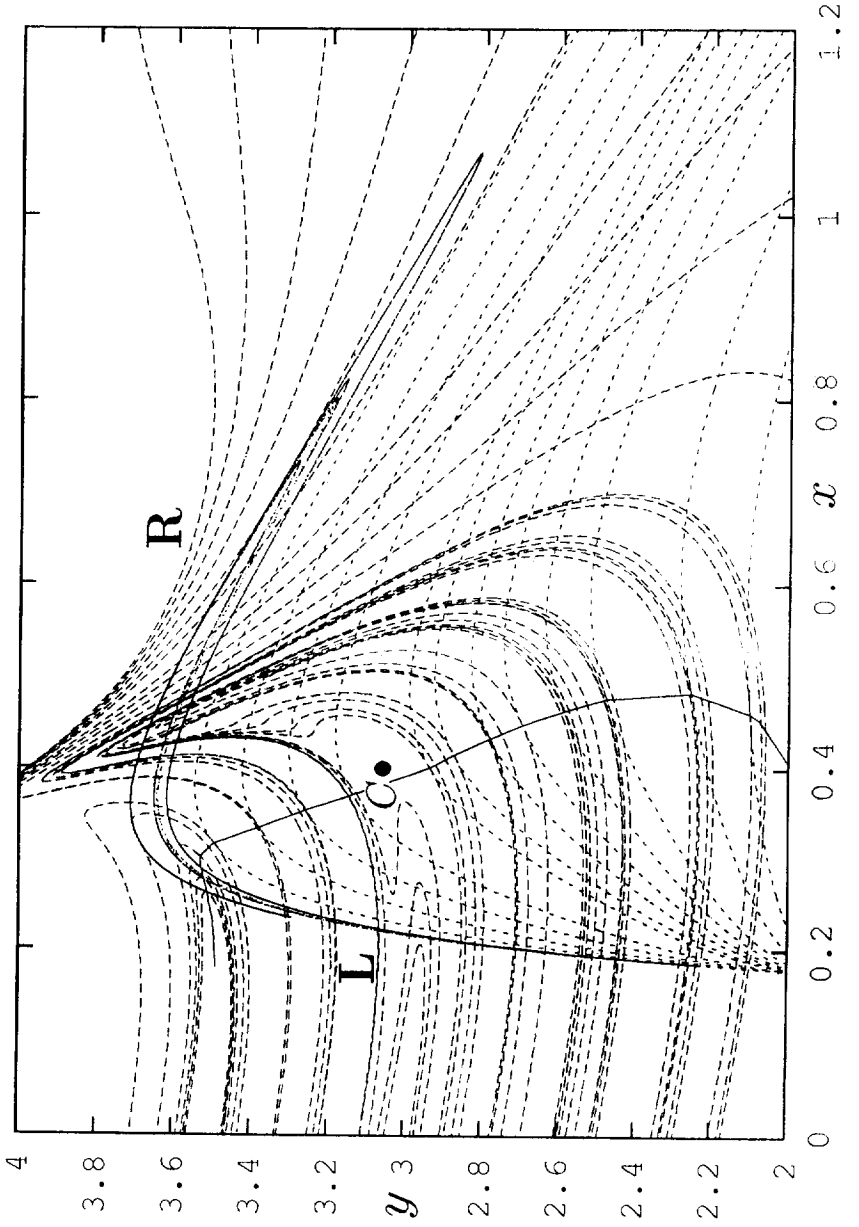

Fig. 15. The chaotic attractor, FCF (dashed lines), BCF (dotted lines), and the partition line C● at $\omega = 0.705$.

where

$$\mu_i = \begin{cases} 0 \\ 1 \end{cases} \quad \text{if} \quad \prod_{j=1}^{i} \epsilon_j = \begin{cases} 1, \\ -1. \end{cases} \tag{23}$$

Similarly, to each backward sequence $\ldots s_{\bar{m}} \ldots s_{\bar{2}} s_{\bar{1}} \bullet$ we assign a real number β:

$$\beta = \sum_{i=1}^{\infty} \nu_i 2^{-i}, \tag{24}$$

where

$$\nu_i = \begin{cases} 0 \\ 1 \end{cases} \quad \text{if} \quad \prod_{j=1}^{i} \epsilon_j = \begin{cases} 1, \\ -1. \end{cases} \tag{25}$$

According to these definitions we have

$$\begin{aligned} &\alpha(\bullet \mathrm{RL}^{\infty}) = \beta(\mathrm{L}^{\infty}\mathrm{R}\bullet) = 1, && \alpha(\bullet \mathrm{L}^{\infty}) = \beta(\mathrm{L}^{\infty}\bullet) = 0, \\ &\alpha(\bullet \mathrm{RRL}^{\infty}) = \alpha(\bullet \mathrm{LRL}^{\infty}) = 1/2, && \beta(\mathrm{L}^{\infty}\mathrm{RR}\bullet) = \beta(\mathrm{L}^{\infty}\mathrm{RL}\bullet) = 1/2. \end{aligned} \tag{26}$$

In the symbolic plane, spanned by α and β, forward and backward foliations become vertical and horizontal lines, respectively. All forward (resp. backward) sequences may be ordered according to their α (resp. β) values. The ordering rule may also be formulated as follows:

$$\begin{aligned} &\bullet \mathrm{ER} \ldots > \bullet \mathrm{EL} \ldots, && \bullet \mathrm{OR} \ldots < \bullet \mathrm{OL} \ldots, \\ &\ldots \mathrm{RE}\bullet > \ldots \mathrm{LE}\bullet, && \ldots \mathrm{RO}\bullet < \ldots \mathrm{LO}\bullet, \end{aligned} \tag{27}$$

where the finite string E (resp. O) consists of letters R and L and contains an Even (resp. Odd) number of the letter R. The ordering rule (27) turns out to be the same as that of the Hénon map with a *positive* Jacobian. For the Hénon map with a positive Jacobian the relations (27) follow from the 'local' ordering, caused by the fact that both eigenvalues of the fixed point R^{∞} (L^{∞}) are negative (positive).

When foliations are well-ordered, the location of a tangency places a restriction on allowed symbolic sequences. A point on the partition line C• may symbolically be represented as QC•P. The rectangle enclosed by the lines QR•, QL•, •P, and $\bullet \mathrm{RL}^{\infty}$ forms a forbidden zone in the symbolic plane. Therefore, a symbolic sequence UV with U• between QR• and QL•, and at the same time •V > •P must be forbidden by the tangency QC•P. In the symbolic plane the sequence UV corresponds to a point inside the forbidden zone of QC•P. Each tangency point on the partition line rules out a rectangle in the symbolic plane. The union of the forbidden rectangles forms the fundamental forbidden zone (FFZ), the left boundary of which is the pruning front [20].

Consider a finite set of tangencies $\{\mathrm{Q}_i\mathrm{C}\bullet\mathrm{P}_i\}$. If the shift of a sequence $\ldots s_{k-2}s_{k-1}\bullet s_k s_{k+1} \ldots$ satisfies the condition that the backward sequence $\ldots s_{k-2}s_{k-1}\bullet$ is not between $\mathrm{Q}_i\mathrm{R}\bullet$ and $\mathrm{Q}_i\mathrm{L}\bullet$, and, at the same time, $\bullet\mathrm{P}_i > \bullet s_k s_{k+1} \ldots$ for some i, then this shift is not forbidden by any tangencies, owing to the property of well-ordering of foliations. Thus, we may say that the shift is allowed according to that tangency. A necessary and sufficient condition for a sequence to be allowed is that all of its shifts are allowed according to the set of tangencies.

In order to check the admissibility condition, we draw 100 000 points representing real sequences generated from the Poincaré map together with the FFZ in the symbolic plane in Fig. 16. Indeed, the FFZ contains no point of allowed sequences. At first glance, the pruning front seems to be a straight line. A blow-up in the α direction shows the

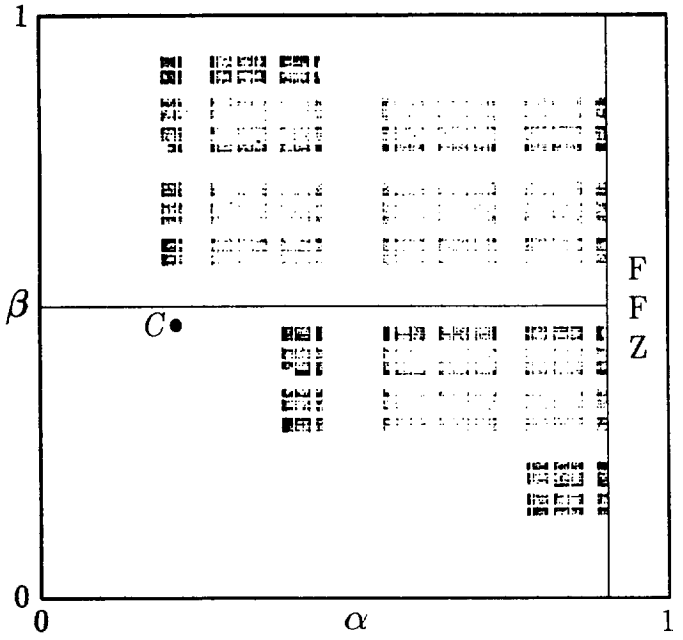

Fig. 16. The symbolic plane at $\omega = 0.705$. A total of 100000 points representing real orbits are drawn together with the FFZ. No point falls in the FFZ.

'structure', displayed in Fig. 17. Note that the α range of Fig. 17 is [0.9022, 0.9032] and the structure shows off in even narrower range. The width of the FFZ steps in α may be taken as an indicator of how good a one-dimensional symbolic dynamics will capture the dynamics of the higher-dimensional system.

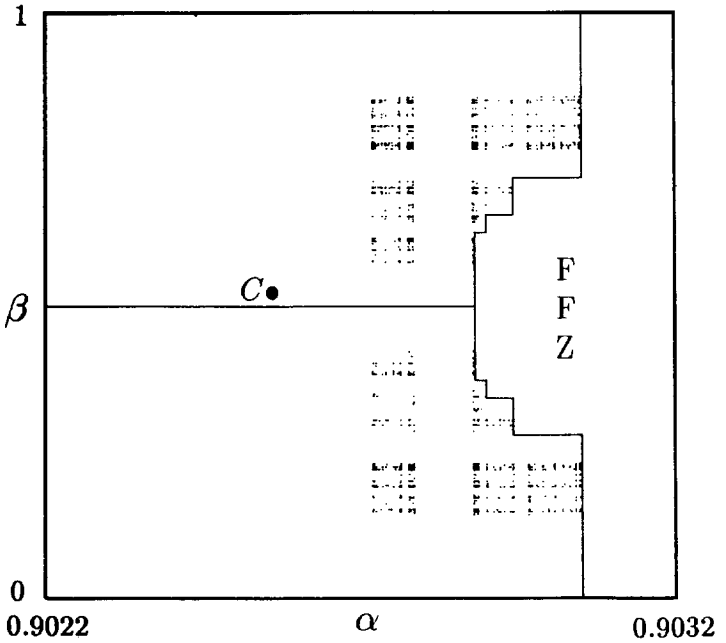

Fig. 17. A blow-up of the symbolic plane Fig. 16 in the interval $\alpha = [0.9022, 0.9032]$.

In the one-dimensional unimodal map there are 802 admissible periodic sequences from C to $(RLLRC)^\infty$ with periods less than or equal to 17, as may be verified by direct generation of these words. Using the six tangencies, listed in the beginning of this section, one may check their admissibility in the forced Brusselator at $\omega = 0.705$. The results are partially listed in Table 3. A short-hand notation is used in the table. If the k-th shift of a periodic sequence $P^\infty \bullet P^\infty$ is allowed or forbidden by a tangency T, we write the criterion as kT or $k\bar{T}$, respectively. In addition, $(0 \ldots n)T = 0T1T \ldots nT$.

First, all sequences from C to RL^2RLRL^2RLC are allowed by T_1. They correspond to the horizontal C• in Fig. 16 or 17. We have shown only the last period 11 in the first row of Table 3. Second, all sequences greater than the period 12 in the next to last row of Table 3 are ruled out by T_6, taken as the kneading sequence in a one-dimensional map. Only in between these two limits two-dimensional symbolic dynamics is essential in telling the admissibility of symbolic sequences. A case which exhibits two-dimensional features more clearly was studied in Ref. [23].

Now we are in a position to treat problems like the missing 6P orbit $(RL^3RC)^\infty$, which was mentioned in Section 2. It was the only missing member in the first U-sequence ever reported in an ODE, when a numerical study was carried out up to period 6 orbits [12]. At $\omega = 0.705$ the $\bullet(RL^3RC)^\infty$ sequence is bigger than the forward sequence in the tangency T_6, which lies at the border of the attractor as its backward sequence $L^\infty C\bullet$ suggests. The same happens at $\omega = 0.8086$ when

$$T_6\text{: } L^\infty C\bullet RL^3(RLR)^2L^2R^2L^3RLR^2L^2R^2 \ldots \qquad (0.222\,703\,913\,2,\ 3.894\,651\,919\,3).$$

Therefore, in order to check the existence of $(RL^3RC)^\infty$ we have to increase ω further. At $\omega = 0.813$ we have found the following tangencies, among others:

$$T_1\text{: } L^\infty RC\bullet R^2LR^2L^3R^4L^2RLR^2LR \ldots \ (0.306\,175\,384\,6,\ 3.751\,890\,561\,9)$$

Table 3. Admissibility of some periodic sequences not greater than $(RLLRC)^\infty$ at $\omega = 0.705$

Sequence	Period	Admissibility	Criterion
RLLRLRLLRLC	11	allowed	$(0 \ldots 10)T_1$
RLLRLRLLRLRRLLRLC	17	allowed	$0T_3(1 \ldots 16)T_1$
RLLRLRLLRLRRLC	14	allowed	$0T_3(1 \ldots 13)T_1$
RLLRLRLLRLRRLRRLC	17	allowed	$0T_3(1 \ldots 16)T_1$
RLLRLRLLRLRRLRRC	16	allowed	$0T_3(1 \ldots 15)T_1$
RLLRLRLLRLRRLRRRC	17	forbidden	$0\bar{T}_2$
RLLRLRLLRLRRLRC	15	forbidden	$0\bar{T}_2$
RLLRLRLLRLRRLRLRC	17	forbidden	$0\bar{T}_2$
RLLRLRLLRLRRLRLC	16	allowed	$0T_5(1 \ldots 15)T_1$
RLLRLRLLRLRRC	13	forbidden	$0\bar{T}_4$
RLLRLRLLRLRRRRLC	16	allowed	$0T_5(1 \ldots 15)T_1$
RLLRLRLLRLRRRRLRC	17	forbidden	$0\bar{T}_4$
RLLRLRLLRLRRRRC	15	forbidden	$0\bar{T}_4$
RLLRLRLLRLRRRRRRC	17	forbidden	$0\bar{T}_4$
RLLRLRLLRLRRRRRC	16	forbidden	$0\bar{T}_4$
RLLRLRLLRLRRRRRLC	17	allowed	$0T_5(1 \ldots 16)T_1$
RLLRLRLLRLRRRC	14	forbidden	$0\bar{T}_4$
RLLRLRLLRLRRRLRLC	17	allowed	$0T_5(1 \ldots 16)T_1$
RLLRLRLLRLRRRLRC	16	forbidden	$0\bar{T}_4$
RLLRLRLLRLRRRLRRC	17	forbidden	$0\bar{T}_4$
RLLRLRLLRLRRRLC	15	allowed	$0T_5(1 \ldots 14)T_1$
RLLRLRLLRLRC	12	forbidden	$0\bar{T}_6$
RLLRC	5	forbidden	$0\bar{T}_6$

C stands for either L or R. Only non-repeating strings of the sequences are given. For the short-hand notation in the 'Criterion' column see text.

T_2: $L^{\infty}RL^2RC\bullet R^2LR^2L^3R^4LR^2L^3R^2$ . . . (0.304 627 269 6, 3.752 397 421 4)

T_3: $L^{\infty}R^2LRC\bullet R^2LR^2LR^2L^2RL^3RL^3R^2$ . . . (0.303 475 017 5, 3.755 752 594 0)

T_4: $L^{\infty}R^2LR^2C\bullet RL^3RLR^2L^2R^2L^3R^4L$ . . . (0.279 680 026 4, 3.903 668 015 6)

T_5: $L^{\infty}R^2C\bullet RL^3RLR^2LR^2L^3R^4L^2$ . . . (0.279 230 515 2, 3.905 714 160 3)

T_6: $L^{\infty}C\bullet RL^3R^2LRL^3RLR^2L^2RL^2$ . . . (0.228 000 592 9, 3.907 657 139 1).

(We use the same notations T_i. This will not cause confusion as ω is indicated.) Now T_6 alone cannot either exclude or justify the existence of $(RL^3RC)^{\infty}$, but T_5 does forbid it. At $\omega = 0.821$ the relevant tangencies are:

T_1: $L^{\infty}RC\bullet R^2L^2R^2L^3R^2L^2R^2L^3R^2$ . . . (0.298 921 874 8, 3.765 433 393 8)

T_2: $L^{\infty}RL^2RC\bullet R^2L^2R^2L^3R^2L^2R^2L^3RL$ . . . (0.298 891 102 1, 3.765 511 029 2)

T_3: $L^{\infty}RL^2R^2LRC\bullet R^2LR^2L^3R^2L^2R^2L^3R^2L$ . . . (0.293 730 077 8, 3.778 573 024 8)

T_4: $L^{\infty}R^2LR^2C\bullet RL^3R^2LRL^3R^4L^2R^2L$ . . . (0.270 273 520 9, 3.940 527 446 6)

T_5: $L^{\infty}C\bullet RL^3R^2L^3RLR^2L^3RLR^2$ . . . (0.218 389 565 3, 3.947 673 904 6).

Now both T_3 and T_4 exclude the $(RL^3RC)^{\infty}$ sequence, but T_5 does nothing. The situation becomes clearer when we draw the foliations, going through the two tangencies. In Fig. 18 the diamond indicates the tangency T_3 and the square T_4. Dash lines show

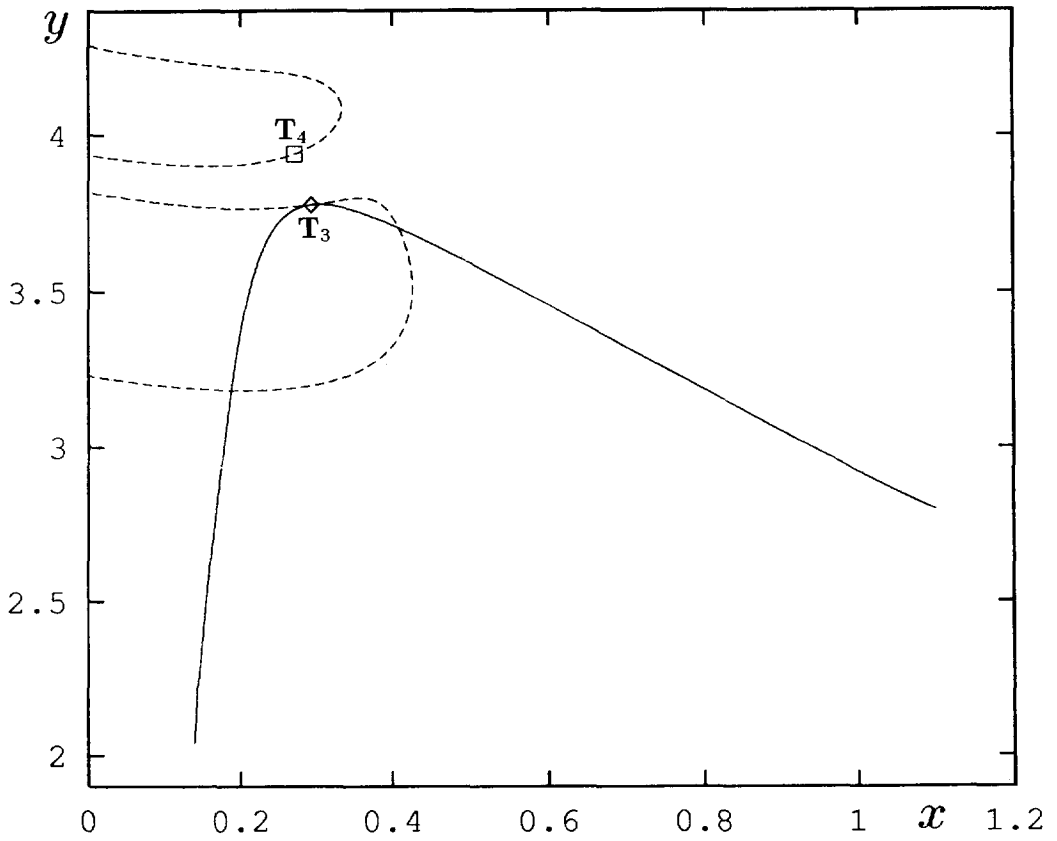

Fig. 18. The forward foliations (dash lines) of the tangencies T_3 (diamond) and T_4 (square) and the backward foliation (solid line) of T_3 at $\omega = 0.821$.

the forward foliations through T_3 and T_4, and the solid line represents the backward foliation of T_3.

According to the order rule (27), the forward foliations associated with $\bullet(RL^3RC)^n \ldots$, $n = 2, 3, \ldots$, must be located in the region between the two forward foliations of T_3 and T_4. At the same time, the backward foliation associated with the sequences $\ldots (RRL^3R)^nC\bullet$ and $\ldots (LRL^3R)^nC\bullet$ necessarily lie in the region below the backward foliation of T_3. Consequently, they are separated by the foliations of T_3. This leads to the non-existence of $(RL^3RC)^n\bullet(RL^3RC)^n$, $(n \to \infty)$.

The foregoing discussion clearly shows that the periodic sequence $(RL^3RC)^\infty$ is always forbidden as ω varies, i.e. the 'missing' period six RL^3RC actually does not exist.

In this way we have checked the U-sequence in the periodically forced Brusselator up to period 7. The results are listed in Table 4. This is to be compared with the early numerical results of 1983 [12]. Now instead of 'missing' we are able to say firmly which orbits are forbidden. This kind of results can never be obtained either by numerical work or by analytical arguments. It also tells the necessity of invoking two-dimensional symbolic dynamics in exploring global behaviour of ODEs.

Before concluding this section, we note that one should be aware of some subtleties which may impede a straightforward symbolic dynamics analysis. For example, behind the seemingly regular pattern of the bifurcation diagram in Fig. 14 some qualitative changes take place in the behaviour of short periodic orbits, which may affect the overall dynamics.

Usually the dynamics on a chaotic attractor is largely dictated by short unstable periodic orbits, say, the fixed point and period 2 orbits (1P and 2P). This is the case at $\omega = 0.79$ or smaller. When $\omega = 0.8015$ and higher, 1P and 2P orbits lie definitely outside the chaotic attractor. The unstable 2P may be further 'swallowed' by 1P. (This is to be distinguished from the case when a *stable* 2P merges into a stable 1P in an inverse period-doubling cascade, as often encountered in the discussion of 'antimonotonicity' of period-doublings.)

The 2P orbit exhibits some more even subtle change. We sketch this in Fig. 19. The

Table 4. Periodic windows along the $A = 0.46 - 0.2\omega$ line in Fig. 1

Word	Period	Range in ω	Width of the window
C†	1	0–0.368 522 4	0.368 522 4
RC	2	0.368 6–0.555 489	0.186 889
RLRC	4	0.555 5–0.577 7	0.022 2
RLRRRC	6	0.582 49–0.582 51	0.000 02
RLRRRRC†	7	0.582 989 983 4–0.582 991 029 838	0.000 001 046 438
RLRRC	5	0.584 5–0.584 8	0.000 3
RLRRLRC†	7	0.588 405 805 31–0.588 458 188 7	0.000 052 383 39
RLC	3	0.594 7–0.654	0.059 3
RLLRLC	6	0.654 5–0.702 5	0.048
RLLRLRC†	7	0.702 993 8–0.703 028 1	0.000 034 3
RLLRC	5	0.706 8–0.711 5	0.004 7
RLLRRRC†	7	0.714 386 619 36–0.714 445 3	0.000 058 680 64
RLLRRC	6	0.718–0.718 5	0.000 5
RLLRRLC†	7	0.721 559 986 71–0.721 727 07	0.000 167 083 29
RLLC	4	0.732 5–0.792	0.059 5
RLLLRLC	7	0.803 5–0.805 6	0.002 1
RLLLRC	6	forbidden	
RLLLRRC	7	0.819 381 023 7–0.819 659 13	0.000 278 106 3
RLLLC	5	0.825 9–0.867 5	0.038
RLLLLRC†	7	forbidden	
RLLLLC	6	0.901 5–0.923	0.021 5
RLLLLLC	7	0.959–0.974	0.015

†Added by us as compared to the U-sequence published in Ref. [12].

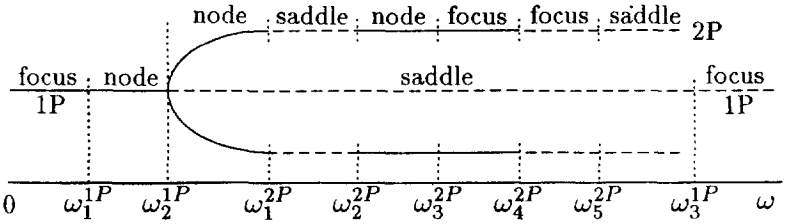

Fig. 19. A sketch of orbital stability transitions of 1P and 2P along the $A = 0.46 - 0.2\omega$ line (not to scale). Solid and dashed lines indicate stable and unstable orbits, respectively.

transition points have been determined numerically: $\omega_1^{1P} = 0.2002249$, $\omega_2^{1P} = 0.36852283$, $\omega_3^{1P} = 0.8202573$, $\omega_1^{2P} = 0.5554892$, $\omega_2^{2P} = 0.7901221$, $\omega_3^{2P} = 0.7901319$, $\omega_4^{2P} = 0.793061175374\,76$, $\omega_5^{2P} = 0.8162116$. Numerical investigation reveals that the orbital stability transitions of 4P is similar to that of 2P.

It is worthy of note that a secondary Hopf bifurcation (also called a Neimark or flutter bifurcation [22]) takes place at ω_4^{2P}. In Table 5 we list the complex conjugate eigenvalues ($\lambda_\pm$) and their moduli ($|\lambda|$) of the 2P orbit in the vicinity of ω_4^{2P}. The determinant J of the linearized stability matrix of 2P is also given. The relations among these quantities are $J = \lambda_+\lambda_-$ and $|\lambda| = \sqrt{(\lambda_+\lambda_-)}$ or $\lambda_\pm = |\lambda| e^{\pm i\phi}$ where $\phi = \tan^{-1}(\mathrm{Im}\,\lambda/\mathrm{Re}\,\lambda)$. As seen from Table 5, when ω crosses ω_4^{2P}, $|\lambda|$ crosses 1. In other words, when ω varies from 0.793 04 to 0.793 08 the complex eigenvalues cross the unit circle in the complex plane at an angle $\phi \neq 0, \pi$.

The Neimark bifurcation is a bit more complicated than the analogous Hopf bifurcation from a fixed point. A limit torus appears instead of a limit cycle. The motion on such a limit torus is quasiperiodic.

7. CONCLUSIONS

We have shown that numerical study under the guidance of symbolic dynamics provides a powerful means to explore the global property of ODEs in their phase and parameter spaces. This combined use of numerical and topological methods yield results that cannot be obtained either by purely numerical search or by entirely analytical arguments. So far, this method has been applied to the analysis of the NMR-laser chaos model [24], the two-well Duffing equation [25], in addition to the forced Brusselator (present work and [23]) and the Lorenz model [4]. We hope it will be used more widely in the future.

As the periodically forced Brusselator is concerned, the transition from annular to interval dynamics has enabled us to trace how the symbolic dynamics evolves from that of 1D circle map to 1D unmodal map via the 2D dissipative standard map and 2D Hénon map. Although some deeper questions, e.g. the analysis of the transition from the U-sequence in the 1D unimodal map to the Farey sequence in the circle map, remain to be tackled, it has furnished a framework for the study of other periodically driven systems.

In addition we have analyzed an interesting case of Neimark bifurcation in the forced

Table 5. The eigenvalues ($\lambda_\pm$) and their moduli ($|\lambda|$) of 2P orbit at and close to ω_4^{2P}

ω	J	$\lambda_\pm$	$\lvert\lambda\rvert$
0.793 04	0.999 361 127 8	$-0.712\,465\,466\,6 \pm 0.701\,251\,799\,9$i	0.999 680 512 9
ω_4^{2P}	1.000 000 000 0	$-0.710\,670\,019\,3 \pm 0.703\,525\,496\,1$i	1.000 000 000 0
0.793 08	1.000 568 270 4	$-0.709\,073\,677\,6 \pm 0.705\,537\,235\,1$i	1.000 284 094 8

Brusselator and elucidated some subtle changes in unstable short periods. The case when unstable 1P and 2P get out of the attractor shows once more the necessity to invoke the tangencies between the forward and backward foliations for the determination of partition lines in two-dimensional symbolic dynamics.

Acknowledgement—This work was partially supported by the National Natural Science Foundation of China. Inspiring discussions with Drs F.-G. Xie and Z.-B. Wu are also gratefully acknowledged.

REFERENCES

1. B.-L. Hao, *Physica* **A140**, 85 (1986).
2. B.-L. Hao, *Elementary Symbolic Dynamics and Chaos in Dissipative Systems*. World Scientific, Singapore (1989).
3. M.-Z. Ding and B.-L. Hao, *Commun. Theor. Phys.* **9**, 375–389 (1988).
4. H.-P. Fang and B.-L. Hao, Symbolic dynamics of the Lorenz equations. *Chaos, Solitons & Fractals* (in press).
5. P. Grassberger and H. Kantz, *Phys. Lett.* **A113**, 235 (1985).
6. W.-M. Zheng, *Chaos, Solitons & Fractals*, **1**, 243 (1991); **2**, 461 (1992); H. Zhao and W.-M. Zheng, *Commun. Theor. Phys.* **19**, 21 (1993).
7. J. J. Tyson, *J. Chem. Phys.* **58**, 3919 (1973).
8. T. Kai and K. Tomita, *Progr. Theor. Phys.* **61**, 54 (1979).
9. K. Tomita and T. Kai, *J. Stat. Phys.* **21**, 65 (1979).
10. B.-L. Hao and S.-Y. Zhang, *Phys. Lett.* **A87**, 267 (1982).
11. B.-L. Hao and S.-Y. Zhang, *J. Stat. Phys.* **28**, 769 (1982).
12. B.-L. Hao, G.-R. Wang and S.-Y. Zhang, *Commun. Theor. Phys.* **2**, 1075 (1983).
13. N. Metropolis, M. L. Stein and P. R. Stein, *J. Combinat. Theor.* **A15**, 25 (1973).
14. G.-R. Wang, S.-G. Chen and B.-L. Hao, *Chin. Phys. (AIP)* **4**, 284 (1983).
15. G.-R. Wang and B.-L. Hao, *Acta Phys. Sinica* **33**, 1321 (1984).
16. W.-M. Zheng, *Int. J. Mod. Phys.* **5B**, 481 (1991); *Chaos, Solitons & Fractals* **4**, 1221 (1994).
17. W.-M. Zheng, Symbolic dynamics of the piecewise linear standard map, preprint.
18. J. M. Greene, *Long-Time Prediction in Dynamics*, edited by W. Horton, L. Reichl and V. Szebehely. Wiley, New York (1983).
19. Y. Gu, *Phys. Lett.* **A124**, 340 (1987).
20. P. Cvitanović, G. H. Gunaratne and I. Procaccia, *Phys. Rev.* **A38**, 1503 (1988).
21. R. Ito, *Math. Proc. Camb. Phil. Soc.* **89**, 107 (1981).
22. J. M. T. Thompson and H. B. Steward, *Nonlinear Dynamics and Chaos*, p. 153. John Wiley and Sons, New York (1986).
23. J.-X. Liu and W.-M. Zheng, *Commun. Theor. Phys.* **23**, 315 (1995).
24. W.-M. Zheng and J.-X. Liu, *Phys. Rev.* **E51**, 3735 (1995).
25. F.-G. Xie, W.-M. Zheng and B.-L. Hao, *Commun. Theor. Phys.* **24**, 43 (1995).